

# Inertial Brownian motors driven by biharmonic signals<sup>☆</sup>

Lukasz Machura<sup>a</sup>, Marcin Kostur<sup>a</sup>, Jerzy Łuczka<sup>a,\*</sup>

<sup>a</sup>*Institute of Physics, University of Silesia, 40–007 Katowice, Poland*

---

## Abstract

We study transport properties of an inertial Brownian particle moving in viscous symmetric periodic structures and driven by an oscillating signal of two harmonic components. We analyze the influence of symmetric, antisymmetric and asymmetric signals on directed transport and reveal the shift symmetry of the stationary averaged velocity of the Brownian particle with respect to the relative phase of two components of the signal. The shift symmetry holds true in all regimes.

*Keywords:* transport, Brownian motors, Josephson junctions

*PACS:* 05.60.Cd, 05.40. a, 05.45. a

---

## 1. Introduction

Recent progress in the highly controlled fabrication of small structures opens new prospects for miniaturization of devices, machines, engines, etc. Processes in such systems can exhibit radically different properties than at the macroscopic level. For example at the microscopic scale, immanently there is a world of fluctuations which cannot be eliminated or even reduced. However, it can be exploited. A good example are biological motors like kinesin or dynein which exploit thermal fluctuations for their directed movement by the ratchet mechanism [1]. At the microscopic or mesoscopic levels, ways and means of generation and control of particle transport are important issues for both theorists [2] and experimentalists [3]. In literature, there are many suggestions and examples how to generate a directed movement of particles [2, 4]. Much more difficult problem is related to a precise control of transport. In the paper, we study an archetype of transport in (spatially) periodic systems which is described by a Langevin equation. In this modeling, we know what conditions have to be fulfilled in order to generate a directed motion of a Brownian particle. Moreover, properties of this system can be experimentally verified in a setup consisting of a resistively and capacitively shunted Josephson junction

device [5, 6, 7]. It is possible because the underlying dynamics can conveniently be described by an equivalent equation of motion in the Stewart-McCumber model [8, 9, 10, 11]. In our previous papers [5, 6], we have studied the system driven by a time-periodic force  $G(t)$  which is the simplest harmonic signal  $G(t) = A \cos(\Omega t)$  (or  $G(t) = A \sin(\Omega t)$ ), where  $A$  and  $\Omega$  are the amplitude and angular frequency of the signal, respectively. We have shown that, when additionally a constant force  $F$  is applied, anomalous transport in experimentally wide regimes can be observed: absolute negative mobility near zero value of  $F$  (a linear response regime), negative mobility in the nonlinear response regime and negative differential mobility. In this paper we extend the analysis by considering the biharmonic driving. However, we assume that the constant force  $F = 0$ .

The paper is organized as follows. In Sec. 2, we present the Langevin equation determining dynamics of the Brownian particle in presence of  $\delta$ -correlated thermal fluctuations. Next, in Sec. 3, we address the problem of influence of the second harmonics on transport of the Brownian particle. In the parameter space, we reveal reach transport behavior. Sec. 4 provides summary and some conclusions.

## 2. Langevin dynamics

We study the motion of a classical particle of mass  $m$  moving in the periodic, symmetric one-dimensional potential  $V(x) = \Delta V \sin(2\pi x/L)$  of the period  $L$  and a

---

<sup>☆</sup>On the occasion of 60th birthday of Prof. Peter Hänggi

\*Corresponding author.

*Email address:* jerzy.luczka@us.edu.pl (Jerzy Łuczka)

*URL:* fizyka.us.edu.pl (Jerzy Łuczka)

54 barrier height  $2\Delta V$ . The particle is driven by an unbi- 92  
 55 ased time-periodic *biharmonic* force 93

$$G(t) = A[\sin(\Omega t) + \epsilon \sin(2\Omega t + \phi)], \quad (1) \quad 94$$

56 where  $\epsilon$  is the ratio of the second harmonic amplitude 95  
 57 to the fundamental amplitude  $A$  and the relative phase  $\phi$  96  
 58 determines the time symmetry of the system. Addition- 97  
 59 ally, the particle is subjected to the thermal noise. Dy- 98  
 60 namics of a such defined Brownian motor is governed 99  
 61 by the Langevin equation for the coordinate  $x = x(t)$  of 100  
 62 the Brownian particle which has the form [12] 101

$$m\ddot{x} + \gamma\dot{x} = -V'(x) + G(t) + \sqrt{2\gamma kT} \xi(t), \quad (2) \quad 102$$

63 where the dot denotes a differentiation with respect to 104  
 64 time and prime denotes a differentiation with respect to 105  
 65 the argument of the potential  $V(x)$ . The parameter  $\gamma$  is 106  
 66 the friction coefficient,  $T$  denotes temperature, and  $k$  is 107  
 67 the Boltzmann constant. Thermal fluctuations are mode- 108  
 68 led by the zero-mean Gaussian white noise  $\xi(t)$  with 109  
 69 the correlation function  $\langle \xi(t)\xi(s) \rangle = \delta(t-s)$ . 110

70 We introduce dimensionless variables. The natural 111  
 71 length scale is determined by the period  $L$  of the poten- 112  
 72 tial  $V(x)$ . The dynamics possesses several time scales. 113  
 73 We define the characteristic time  $\tau_0$  determined from 114  
 74 the Newton equation,  $m\ddot{x} = -V'(x)$ , by inserting char- 115  
 75 acteristic quantities, namely,  $mL/\tau_0^2 = \Delta V/L$ ; hence 116  
 76  $\tau_0^2 = mL^2/\Delta V$ . The dimensionless variables thus read: 117

$$\hat{x} = \frac{x}{L}, \quad \hat{t} = \frac{t}{\tau_0}. \quad (3) \quad 118$$

77 The dimensionless Langevin dynamics consequently 119  
 78 assumes the form 120

$$\ddot{\hat{x}} + \hat{\gamma}\dot{\hat{x}} = -\hat{V}'(\hat{x}) + g(\hat{t}) + \sqrt{2\hat{\gamma}D_0} \hat{\xi}(\hat{t}), \quad (4) \quad 121$$

80 where 122

- 81 • the re-scaled friction coefficient  $\hat{\gamma} = (\gamma/m)\tau_0$  is the 123  
 82 ratio of the two characteristic time scales,  $\tau_0$  and 124  
 83 the relaxation time scale of the velocity degree of 125  
 84 freedom, i.e.,  $\tau_L = m/\gamma$ , 126
- 85 • the re-scaled potential 127

$$\hat{V}(\hat{x}) = V(x)/\Delta V = \sin(2\pi\hat{x}) \quad (5) \quad 128$$

86 assumes the period 1 and the barrier height 2, 129

- 87 • the scaled external time-periodic force 130

$$g(\hat{t}) = a[\sin(\omega\hat{t}) + \epsilon \sin(2\omega\hat{t} + \phi)] \quad (6) \quad 131$$

88 where the signal has the re-scaled amplitudes  $a = 132$   
 89  $AL/\Delta V$  and  $\epsilon = \epsilon/\Delta V$  and the dimensionless an- 133  
 90 gular frequencies  $\omega = \Omega\tau_0$ , 134

- the re-scaled, zero-mean Gaussian white noise 135  
 forces  $\hat{\xi}(\hat{t})$  obey  $\langle \hat{\xi}(\hat{t})\hat{\xi}(\hat{s}) \rangle = \delta(\hat{t}-\hat{s})$  with a re-scaled 136  
 noise intensity  $D_0 = kT/\Delta V$ . 137

In the following, mostly for the sake of simplicity, we shall use only dimensionless variables and shall omit the “hat”-notation in all quantities.

Transport properties in systems driven by this type of external stimulus have been theoretically studied mainly in the overdamped regime [13, 14, 15], for moderate damping [16], both experimentally and theoretically for cold atoms in the optical lattices [17, 18, 19], and for driven Josephson junctions [20].

### 3. Influence of the second harmonic of the driving

From the symmetry considerations it follows that the long-time averaged velocity  $v$  of the Brownian motor is equal to zero if it is driven only by one harmonic, i.e. when  $\epsilon = 0$  in Eq. (6). In order to generate a directed motion of the motor, one has to include the second harmonic. Therefore we pose here the question: what is the influence of the second component ( $\epsilon \neq 0$ ) of the external force  $g(t)$  on transport properties of the Brownian particle described by Eq. (4).

Nonlinearity and three-dimensional phase space ( $x, y = \dot{x}, z = \omega t$ ) make the system (4) possible to behave chaotically in the deterministic case ( $D_0 = 0$ ). Many features depend strongly on the shape of basins of attraction. If we however plug the temperature on, it is very likely that we destroy the present scene of attractors and release the possibility for the system to proceed not only with attractors but more importantly with the deterministic unstable orbits. This situation is extremely complicated and can change from point to point in the five-dimensional parameter space  $\{\gamma, \omega, a, \epsilon, D_0\}$ . It is almost impossible to find all features for such a system; therefore the goal of this work is focused only on the generic influence of the biharmonicity parameter  $\epsilon$ . In fact, one is able to tangle the picture even more by setting the frequency of the second harmonic in  $g(t)$  free, but authors feel that this is unnecessarily in this very work.

In the following we will fix the dimensionless temperature to the value  $D_0 = 0.001$  and focus on the stochastic (not deterministic) properties.

#### 3.1. Numerical experiment

In order to establish the influence of the second harmonic of the driving force on transport properties

138 we have carried out comprehensive numerical simulations.  
 139 We have employed Stochastic Runge–Kutta algorithm of the 2<sup>nd</sup> order with the time step of  $[10^{-3} \div$   
 140  $10^{-4}](2\pi/\omega)$ . All numerical calculations have been performed using CUDA environment on desktop computing  
 141 processor NVIDIA Tesla C1060. This gave us a possibility to speed the numerical calculations up to  
 142 few hundreds times more than on typical modern CPUs. More details on this very efficient method can be found  
 143 in the work [21].

148 We focus on the asymptotic current or long–time averaged velocity  $v$  of the Brownian particle. Averaging  
 149 was performed over  $10^3 - 10^6$  different realizations and over one period of the external driving force  $T = 2\pi/\omega$ .  
 150 We choose all initial positions and velocities to be uniformly distributed over one potential period  $[0, 1]$  and  
 151 the interval  $v \in [-2, 2]$ , respectively.  
 152  
 153  
 154

### 155 3.2. Role of symmetry in time domain

156 Properties of the time dependent driving force  $g(t)$  in Eq. (6) determine whether the Brownian particle is  
 157 transported in the long-time regime, i.e. whether  $v = 0$  or  $v \neq 0$ . We can distinguish two special cases of the  
 158 force  $g(t)$ .  
 159  
 160

161 (i) The first case is when there is such  $t_0$  that  $g(t_0 + t) = g(t_0 - t)$ . It means that the driving is symmetric or invariant  
 162 under the time-inversion transformation, see solid and dotted lines in Fig. 1.  
 163  
 164

165 (ii) The second case is when there is such  $t_1$  that  $g(t_1 + t) = -g(t_1 - t)$ . This is the case of the antisymmetric  
 166 driving, see dashed and dotted-dashed lines in Fig. 1.  
 167  
 168

169 As a consequence, in the symmetric case (i), the stationary average velocity tends to zero when the friction  
 170 coefficient  $\gamma$  tends to zero:  $v \rightarrow 0$  when  $\gamma \rightarrow 0$ ; if  $\gamma \neq 0$  then generically  $v \neq 0$ . It is illustrated in Fig. 2  
 171 for  $\phi = \pi/2, 3\pi/2$ . In the asymmetric case (ii), the stationary average velocity tends to zero when the friction  
 172 coefficient  $\gamma$  tends to infinity (the overdamped regime):  $v \rightarrow 0$  when  $\gamma \rightarrow \infty$ ; if  $\gamma < \infty$  then generically  $v \neq 0$ .  
 173 Let us note that contrary to the symmetric driving, for  $\gamma \rightarrow 0$  the velocity  $v \neq 0$ , cf. Fig. 2. So, it means that  
 174 the transport is generated by deterministic dynamics.  
 175  
 176

179 We consider the case of the symmetric driving with  $\phi = \pi/2$  for the biharmonicity  $\varepsilon = 0.5$  (see Fig. 1) and  
 180 study the role of dissipation characterized by the friction coefficient  $\gamma$ . This is the case when for  $\gamma = 0$  the stationary  
 181 average velocity  $v = 0$ . When the friction coefficient increases starting out from zero, the average velocity be-  
 182 comes non-zero as is illustrated in Fig. 2. The average velocity as a function of  $\gamma$  displays non-monotonic de-  
 183 pendence exhibiting maxima and minima. Moreover, it passes through zero and the current reversal phenomena  
 184  
 185  
 186  
 187  
 188

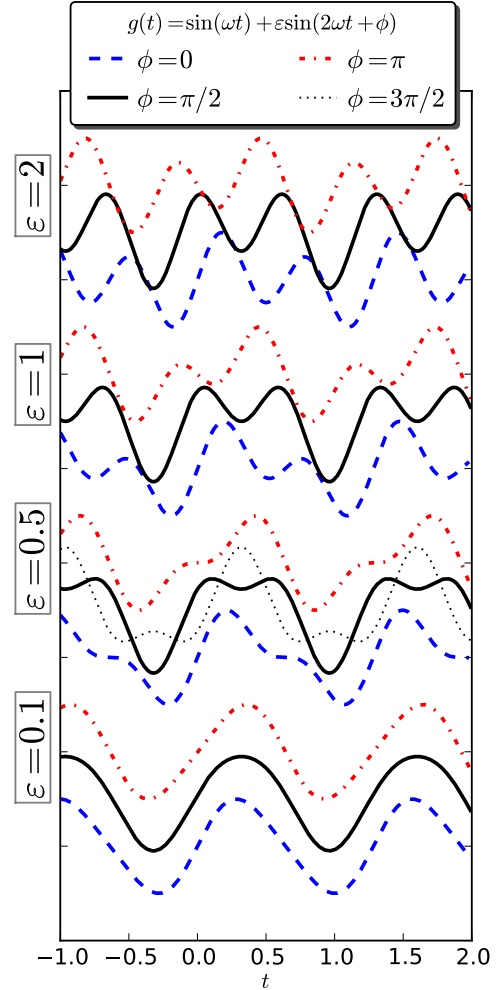


Figure 1: (color online) Dimensionless external ac driving  $g(t) = a[\sin(\omega t) + \varepsilon \sin(2\omega t + \phi)]$  for the fundamental amplitude  $a = 1$ , four different relative amplitudes of the second harmonics:  $\varepsilon = 0.1, 0.5, 1, 2$  and selected values of the relative phase:  $\phi = 0$  (blue dashed),  $\pi/2$  (black solid),  $\pi$  (red dotted-dashed) and  $3\pi/2$  (black dotted). For arbitrary values of  $a$  and  $\varepsilon$ , the ac driving possesses the time reflection symmetry for  $\phi = \pi/2$  and  $\phi = 3\pi/2$ . For  $\phi = 0$  and  $\phi = \pi$  the driving is antisymmetric. For other values of the relative phase  $\phi$  the driving is asymmetric.

189 can be detected. Because for  $\gamma = 0$  the velocity  $v = 0$   
 190 and for  $\gamma \neq 0$  generically the velocity  $v \neq 0$ , this case is  
 191 called the dissipation-induced symmetry breaking [22]:  
 192 the coupling to thermal bath is enough to break the time  
 193 inversion symmetry. We note that for a fixed damping  
 194  $\gamma$ , the average velocity for the phase  $\phi = 3\pi/2$  takes  
 195 exactly the opposite sign to the case  $\phi = \pi/2$ .

196 Now, let us consider the antisymmetric case  $\phi = 0$ .  
 197 For  $\gamma = 0$ , the velocity  $v \neq 0$ . The weak dissipa-  
 198 tion diminishes the stationary velocity in comparison  
 199 to the dissipationless case. The dependence  $v(\gamma)$   
 200 is also non-monotonic with minima and maxima. As in  
 201 the symmetric case, the case with the phase  $\phi = \pi$   
 202 can be obtained from the case  $\phi = 0$  by the relation  
 $v(\phi = \pi) = -v(\phi = 0)$ .

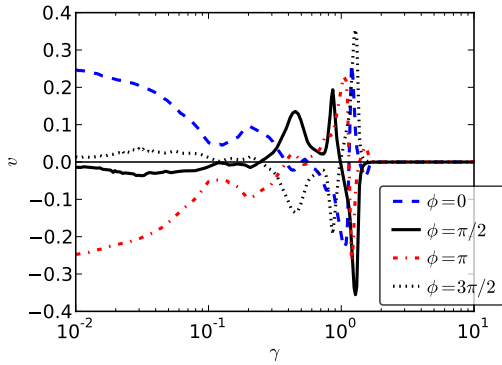


Figure 2: (color online) The stationary average velocity  $v$  as a function of the friction coefficient  $\gamma$  is depicted for selected values of the relative phase  $\phi$ . For  $\phi = \pi/2, 3\pi/2$  the driving is symmetric while for  $\phi = 0, \pi$  it is antisymmetric. Other parameters read:  $a = 4.2$ ,  $\omega = 4.9$ ,  $\varepsilon = 0.5$  and  $D_0 = 0.001$ .

203

### 204 3.3. Arbitrary shape of driving

205 In previous subsection we focused on specific values  
 206 of the phase. Here we present the numerical investiga-  
 207 tion of the 3D parameter space  $\{\phi, \varepsilon, \gamma\}$ . For phases dif-  
 208 ferent than just mentioned above, we reveal also asym-  
 209 metric external biharmonic signals. In the Fig. 3, the  
 210 average velocity is presented in color plots for four dif-  
 211 ferent damping constants  $\gamma = 0.01, 0.1, 0.9, 2$  (panels  
 212 a–d respectively) and additionally for the overdamped  
 213 limit (panel e). On the abscissa we vary the amplitude  $\varepsilon$   
 214 of the second component of the signal  $g(t)$  and on ordi-  
 215 nate we present phase  $\phi \in [0, 2\pi]$ . Light colors denote  
 216 positive average velocity. Color becomes darker for val-  
 217 ues of  $v$  close to zero and eventually turn to dark–gray  
 218 and black for negative valued average velocities.

219 For the weak friction the average velocity has reflec-  
 220 tion symmetry  $v(\pi + \phi) = v(\pi - \phi)$  as we would expect

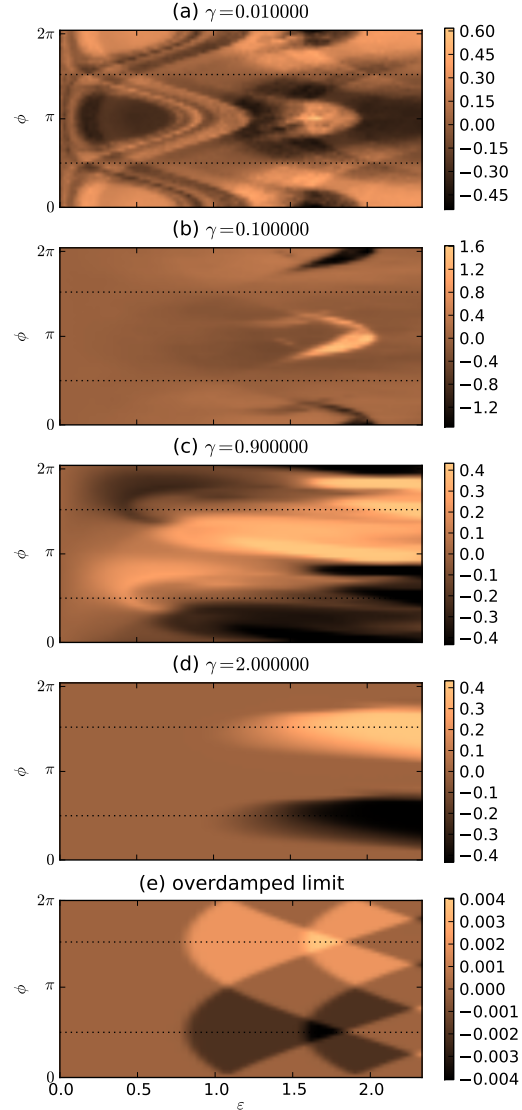


Figure 3: (color online) Influence of the second harmonic of the external force  $g(t)$  on transport properties of the system (4). Dependence of the drift velocity on both the relative amplitude  $\varepsilon$  (horizontal axis) and the relative phase  $\phi$  (vertical axis) is depicted for various damping constants  $\gamma = 0.01, 0.1, 0.9, 2.0$  and for the overdamped limit (top to bottom). Other parameters are:  $a = 4.2$ ,  $D_0 = 0.001$  and  $\omega = 4.9$ . Black dotted lines are plotted on all panels showing the phases for which the driving force  $g(t)$  possesses the reflection symmetry  $t \rightarrow -t$ , i.e. for  $\phi = \pi/2$  and  $3\pi/2$ .

221 from a system prepared very close to the limit of the  
 222 frictionless or Hamiltonian systems, because then the  
 223 relation  $v \approx \sin(\phi + \pi/2)$  is quite well satisfied [23].  
 224 We plotted black dotted lines on each panel to guide the  
 225 reader to the point where the driving force  $g(t)$  possesses  
 226 the reflection symmetry, i.e., for  $\phi = \pi/2$  and  $3\pi/2$ .

227 As we increase the friction coefficient system loses  
 228 its previous symmetry and becomes non-symmetric as  
 229 one can easily see on panels (b) and (c). In other words  
 230 – in the situation where both characteristic times in the  
 231 system  $\tau_\gamma$  and the period  $T$  of the driving take more or  
 232 less the same value, the battle between periodic stimu-  
 233 lation and damping (not strong enough to suppress the  
 234 driving influence quickly with possibility of additional  
 235 energy cumulation) causes the whole irregular dynam-  
 236 ics as seen on the central panel (c) of Fig. 3. If we,  
 237 however, analyze situation with strong damping the pic-  
 238 ture again gains the symmetry but now of a different  
 239 kind, i.e.  $v(\pi + \phi) = -v(\pi - \phi)$ , cf. panel (e) in Fig. 3.  
 240 The close inspection of all case presented in Fig. 2 and  
 241 Fig. 3 leads to the important conclusion that for a fixed  
 242 set of all parameters, there is the shift-symmetry of the  
 243 stationary velocity with respect to the phase, i.e.,

$$v(\phi) = -v(\phi + \pi). \quad (7)$$

244 This relation is a particular case of a more general rela-  
 245 tion

$$v(-\varepsilon) = -v(\varepsilon) \quad (8)$$

246 which follows from the symmetry considerations. One  
 247 can note that the transformation  $\phi \rightarrow \phi + \pi$  is equiva-  
 248 lent to the transformation  $\varepsilon \rightarrow -\varepsilon$ . The same relation  
 249 holds true if, instead of the second harmonics, we apply  
 250 a constant force  $F$ . Then of course  $v(-F) = -v(F)$  [6].  
 251 Remember that for any set of parameters the stationary  
 252 average velocity  $v = 0$  when  $F = 0$  or  $\varepsilon = 0$

### 253 3.4. Controlling transport by symmetric signals

254 We analyze the case when the external driving is sym-  
 255 metric. We set the phase of the second harmonics to  
 256  $\phi = \pi/2$  (see black solid curves in Fig. 1). We check the  
 257 system response to the signal against the relative ampli-  
 258 tude of the second harmonics  $\varepsilon$  for the range start-  
 259 ing from 0 and ending at the value higher than dou-  
 260 bled base driving amplitude  $a$ . In Fig. 4 these char-  
 261 acteristics are plotted for selected driving frequencies  
 262  $\omega = 0.1, 3, 4, 4.9$ . From numerical analysis it follows  
 263 that the average velocity changes its sign by varying the  
 264 parameter  $\varepsilon$  for all inspected frequencies of the exter-  
 265 nal driving. It means that the shape of the external sig-  
 266 nal can control values and direction of the net veloc-  
 267 ity in the system. The current reversal can be multiple

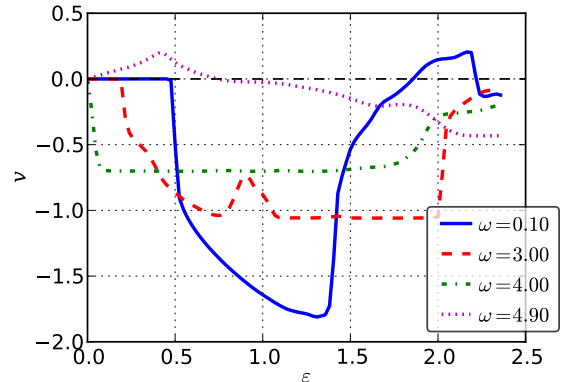


Figure 4: (color online) The stationary averaged velocity  $v$  vs. the relative amplitude  $\varepsilon$  of the second harmonics for four values of the angular frequency  $\omega$  of the signal  $g(t)$ . Other parameters are:  $a = 4.2$ ,  $\gamma = 0.9$ ,  $\phi = \pi/2$  and  $D_0 = 0.001$ .

268 ( $\omega = 0.1$ ), akin to the situation described in [24]. Keep-  
 269 ing  $\varepsilon$  constant at a certain level usually the direction of  
 270 the average motion of Brownian particles changes its  
 271 sign for the different values of the driving frequency  
 272 ( $\varepsilon = 0.5$  or  $2.0$ ). On the contrary there are regimes  
 273 within the scanned parameter space  $\{\varepsilon, \omega\}$  where regard-  
 274 less the values of  $\omega$  chosen the system response is qual-  
 275 itatively the same.

276 Next we explore the transport properties for the  
 277 Brownian particle moving in the viscous environment  
 278 with different friction coefficients. We examine the  
 279 character of the system response against the signal of  
 280 the different shape which we can control by tuning the  
 281 parameter  $\varepsilon$  (see Fig. 1 for details). There are two alter-  
 282 native limits for the viscous system behavior - Hamilto-  
 283 nian where system is frictionless [25, 26, 27] and over-  
 284 damped where the characteristic relaxation time for the  
 285 velocity  $\tau_\gamma = 1/\gamma$  is very long. Between those two pe-  
 286 ripheries there is a region of moderate damping which  
 287 seems to be the most intriguing [5, 6, 28, 29]. It pro-  
 288 vides rich spectrum of the very interesting phenomena  
 289 and therefore we are going to focus on this particular  
 290 domain in the following.

291 In Fig. 5 the reflection of the impact of different  
 292 shapes and strengths of external driving for the friction  
 293 constant  $\gamma$  in the range from 0.1 to 10 can be found.  
 294 This means that the characteristic relaxation time passes  
 295 from 10 to 0.1. If we refer this time to the second char-  
 296 acteristic time of importance for system (4), namely the  
 297 period of the external driving  $T = 2\pi/\omega \simeq 1.28$ , one can  
 298 see that the point where both characteristic times are of  
 299 the same order can be identified more or less in the mid-

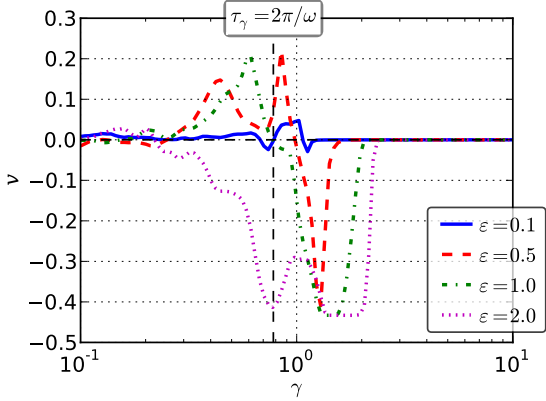


Figure 5: (color online) Logarithmic dependence of the average velocity on the friction coefficient  $\gamma$  is plotted for four relative amplitudes  $\varepsilon$  of the second harmonics of the external driving  $g(t)$ . Vertical black dashed line marks the point of the critical value of the friction coefficient, for which two characteristic times, relaxation time of the velocity  $\tau_\gamma = 1/\gamma$  and period  $T = 2\pi/\omega$  of the driving force, are equal. One can easily notice rich behavior of the average velocity around this specific value. Other parameters are:  $a = 4.2$ ,  $\omega = 4.9$ ,  $\phi = \pi/2$  and  $D_0 = 0.001$ .

dle of the chosen region of analyzed damping constants. Indeed, after examining of Fig. 5, one can easily reveal most exciting features around essential value of the damping constant marked by the vertical dashed black line on the plot. At low friction, the average velocity is close to zero. When we, however, increase the friction coefficient to the value of around  $\gamma = 0.3$  the system starts to react in a different way depending on the relative strength of the second harmonic  $\varepsilon$ . For strengths less then or equal to 1 the current becomes positive, while for  $\varepsilon = 2$  system reacts with the opposite sign. This gives a possibility to control the transport simply by varying the strength of the second source of the external field. When we go even further and arrive to the vicinity of the critical point  $\tau_\gamma = 2\pi/\omega$ , the previous positive valued current starts to drop, crosses zero and becomes negative quite steeply. Surprisingly values of average velocities for all strengths higher than 0.5 possess almost the same negative values just above  $\gamma = 1$ . Additional enlargement of the friction leads to reduce of the transport possibilities of the system. It does not reach zero, but decreases of several orders of magnitude – see panel (e) on Fig. 3 for details. By setting the strength to zero we end up with the antisymmetric force and with zero current for any value of the friction constant due to the symmetry reasons.

## 4. Summary

We have explored transport properties of the Brownian particles in a symmetric potential, driven by the time periodic biharmonic signals. We have demonstrated how the symmetry of driving force influences the transport features. There exists two limits: overdamped and frictionless. It turns out that in those two limits different types of symmetry exclude transport. In the frictionless case the system is time-reversible, thus the symmetric driving cannot distinct the direction. On the other hand, in the case of overdamped motion the antisymmetric driving leads to zero current. In all other cases, as the Curie principle suggests, the particle has generally non-zero average velocity. The closer inspection shows that the magnitude and sign of the current has complex structure in the parameter space. Typically, the multiple current reversals occur, when one of the system parameters is changed.

In this paper, thermal noise  $\xi(t)$  in Eq. (2) is assumed to be white noise of zero correlation time. In real systems the correlation time of thermal fluctuations is never zero. In many situations this approximation is very well but there are also situations where the white-noise approximation fails and a different treatment based e.g. on the generalized Langevin equation should be used [30]. However, it is essentially beyond the scope of the paper and requires separate investigations.

Finally, let us remind that the Langevin equation (2) has similar form as an equation of motion for the phase difference  $\Psi = \Psi(t)$  between the macroscopic wave functions of the Cooper pairs on both sides of the Josephson junction. The quasi-classical dynamics of the resistively and capacitively shunted Josephson junction, which is well known in the literature as the Stewart-McCumber model [8, 9, 11], is described by the following equation

$$\begin{aligned} \left(\frac{\hbar}{2e}\right)^2 C \ddot{\Psi} + \left(\frac{\hbar}{2e}\right)^2 \frac{1}{R} \dot{\Psi} + \frac{\hbar}{2e} I_0 \sin \Psi \\ = \frac{\hbar}{2e} I(t) + \frac{\hbar}{2e} \sqrt{\frac{2k_B T}{R}} \xi(t). \end{aligned} \quad (9)$$

The left hand side contains three additive current contributions: a displacement current due to the capacitance  $C$  of the junction, a normal (Ohmic) current characterized by the normal state resistance  $R$  and a Cooper pair tunnel current characterized by the critical current  $I_0$ . In the right hand side,  $I(t)$  is an external current. Thermal fluctuations of the current are taken into account according to the fluctuation-dissipation theorem and satisfy the Nyquist formula associated with the resistance  $R$ . It is an evident correspondence between two models:

372 the coordinate  $x = \Psi - \pi/2$ , the mass  $m = (\hbar/2e)^2 C$ , the  
 373 friction coefficient  $\gamma = (\hbar/2e)^2 (1/R)$ , the barrier height  
 374  $\Delta V = (\hbar/2e) I_0$  and the period  $L = 2\pi$ . The biharmonic  
 375 signal  $G(t)$  in Eq. (1) corresponds to the external current  
 376  $I(t)$ . The velocity  $v = \dot{x}$  corresponds to the voltage  $V$   
 377 across the junction. So, all transport properties can be  
 378 tested in the setup consisting of a resistively and capac-  
 379 itively shunted Josephson junction device.

### 380 Acknowledgment

381 The work supported in part by the MNiSW Grant  
 382 N202 203534 and the Foundation for Polish Science (L.  
 383 M.). The authors thank M. Januszewski for preparing  
 384 the precise program (<http://gitorious.org/sdepy>) that we  
 385 have used for numerical calculations. We would like to  
 386 acknowledge Peter Hänggi, our friend and mentor, for  
 387 long-term collaboration, inspiring, motivating and never  
 388 ending - not only scientific - discussions.

### 389 References

390 [1] L. Machura, M. Kostur and J. Łuczka, *Biosystems* 94 (2008)  
 391 253.  
 392 [2] P. Hänggi and F. Marchesoni, *Rev. Mod. Phys.* 81 (2009) 387.  
 393 [3] H. Linke, ed., *Ratchets and Brownian motors: Basics, experi-*  
 394 *ments and applications*, Applied Physics A vol. 75 (2002).  
 395 [4] J. Łuczka, R. Bartussek and P. Hänggi, *Europhys. Lett.* 31, 431  
 396 (1995); T. Czernik, J. Kula, J. Łuczka and P. Hänggi, *Phys. Rev.*  
 397 *E.* 55, (1997) 4057; J. Kula, M. Kostur and J. Łuczka, *Chem.*  
 398 *Phys.* 235 (1998) 27.  
 399 [5] L. Machura, M. Kostur, P. Talkner, J. Łuczka and P. Hänggi,  
 400 *Phys. Rev. Lett.* 98 (2007) 040601.  
 401 [6] M. Kostur, L. Machura, P. Talkner, P. Hänggi and J. Łuczka,  
 402 *Phys. Rev. B* 77 (2008) 104509; M. Kostur, L. Machura, J.  
 403 Łuczka, P. Talkner and P. Hänggi, *Acta Phys. Polon. B* 39 (2008)  
 404 1177.  
 405 [7] J. Nagel, D. Speer, T. Gaber, A. Sterck, R. Eichhorn, P.  
 406 Reimann, K. Ilin, M. Siegel, D. Koelle and R. Kleiner, *Phys.*  
 407 *Rev. Lett.* 100 (2008) 217001.  
 408 [8] W.C. Stewart, *Appl. Phys. Lett.* 12, (1968) 277.  
 409 [9] D. E. McCumber, *J. Appl. Phys.* 39, (1968) 3113.  
 410 [10] A. Barone and G. Paternò, *Physics and Application of the*  
 411 *Josephson Effect*, Wiley, New York, (1982).  
 412 [11] R. L. Kautz, *Rep. Prog. Phys.* 59 (1996) 935.  
 413 [12] P. Hänggi and H. Thomas, *Phys. Rep.* 88 (1982) 207.  
 414 [13] M. Borromeo and F. Marchesoni, *Europhys. Lett.* 72 (2005) 362.  
 415 [14] M. Borromeo, P. Hänggi and F. Marchesoni, *J. Phys.: Condens.*  
 416 *Matter* 17 (2005) S3709.  
 417 [15] M. Borromeo and F. Marchesoni, *Phys. Rev. E* 73 (2006)  
 418 016142.  
 419 [16] H. J. Breymayer, *Appl. Phys. A* 33 (1984) 1.  
 420 [17] F. Renzoni, *Cont. Phys.* 46, (2005) 161.  
 421 [18] M. Brown and F. Renzoni, *Phys. Rev. A* 77 (2008) 033405.  
 422 [19] S. Denisov, S. Flach and P. Hänggi, in: *Nonlinearities in Pe-*  
 423 *riodic Structures and Metamaterials*, C. Denz, S. Flach, and Y.  
 424 Kivshar, eds. Springer Series in Optical Sciences vol. 150 (2010)  
 425 181 Springer.  
 426 [20] R. Monaco, *J. Appl. Phys.* 68 (1990) 679.

427 [21] M. Januszewski and M. Kostur, *Comput. Phys. Commun.* 181  
 428 (2010) 183.  
 429 [22] R. Gommers, S. Bergamini and F. Renzoni, *Phys. Rev. Lett.* 95  
 430 (2005) 073003.  
 431 [23] O. Yevtuschenko, S. Flach, Y. Zolotaryuk and A. A. Ovchin-  
 432 nikov, *Europhys. Lett.* 54 (2001) 141.  
 433 [24] M. Kostur and J. Łuczka, *Phys. Rev. E* 63 (2001) 021101.  
 434 [25] H Schanz, MF Otto, R Ketzmerick and T Dittrich, *Phys. Rev.*  
 435 *Lett.* 87 (2001) 070601.  
 436 [26] S. Denisov, S. Flach and P. Hänggi, *Europhys. Lett.* 74 (2006)  
 437 588.  
 438 [27] R Salgado-Garca, M Aldana and G Martnez-Mekler, *Phys. Rev.*  
 439 *Lett.* 96 (2006) 134101.  
 440 [28] L. Machura, M. Kostur, F. Marchesoni, P. Talkner, P. Hänggi  
 441 and J. Łuczka, *J. Phys.: Condens. Matter* 17 (2005) S3741.  
 442 [29] Bao-quan Ai and Liang-gang Liu, *Phys. Rev. E* 76 (2007)  
 443 042103.  
 444 [30] M. Kostur, J. Łuczka and P. Hänggi, *Phys. Rev. E* 80 (2009)  
 445 051121.